Total Pressure Averaging by Small-Diameter Tubes in Pulsating Flows

Zbyszko Kazimierski* and Longin Horodko†
Technical University of Lodz, Lodz, Poland

The problem of the time-averaged pressure of pulsating flow is the subject of this paper. The averaged pressure occurring at the end of the total pressure tube system does not represent the true averaged pressure at the probe inlet. The pulsating flow with significant amplitudes of the total pressure, regarded as being parallel to the total pressure probe axis, is considered. The calculation of the time-averaged pressure inside the total pressure probe is based on the method proposed earlier by the first author. In order to enlarge a practical meaning of the method, it was supplemented with the procedure introducing the entrance effects of the gas motion inside the tube. These effects cause a conversion of a part of the external-stream kinetic energy into an additional total pressure rise in the entrance segment of the tube. The semiempirical method for the quantitative assessment of these effects has been proposed. The available experimental results were compared with those obtained from the theoretical calculations, and a good agreement has been noticed. The pressure correction functions vs frequency were well predicted for all cases under consideration.

Nomenclature

a_0 = mean sound velocity at the tube inlet, m/s
IPD = relative inlet total pressure difference, Eq. (23)
i = imaginary unit, $=\sqrt{-1}$
K = nondimensional parameter, Eq. (11)
k = number of harmonic, k = 1,2. . .
L = tube length, m
P = pressure, N/m^2
Pr = Prandtl number, Eq. (10)
P_0 = true time-averaged pressure, N/m^2
p = nondimensional pressure or pressure perturbations, related to P_0
R = internal tube radius, m
s = shear wave number, Eq. (11)
t = time, s
u,v = nondimensional components of velocity, related to a_o
W = external stream velocity, m/s, Eq. (19)
β = inlet pressure wave coefficient, Eq. (23)
ΔP = pressure amplitude or pressure rise, N/m^2
ϵ = small parameter, Eq. (2)
κ = isentropic expansion index
μ = viscosity, kg/ms
ξ = nondimensional axial coordinate, related to L
ρ = nondimensional density, related to ρ_o
ρ_o = mean density at the tube inlet, kg/m^3
τ = nondimensional time, $=\Omega t$
Ω = frequency, rad/s
ω = nondimensional frequency, Eq. (11)

Subscripts (before comma)
1 = first-order perturbations
1c = real part of 1z
1s = imaginary part of 1z
1z = first-order complex amplitude
20 = second-order time-averaged perturbation or amplitude

Subscript (after comma or single)
j = number of consecutive tube segment

Superscripts
k = number of harmonic
RA = averaged across the tube

Introduction

A COMMON method of measuring the time-dependent pressure is to use special high-frequency miniature pressure transducers. The pulsating pressure is directly sensed by the transducer located in the measurement point. In aerodynamic practice, however, this kind of pressure-measuring device is only a part of the pressure-measuring equipment. Unsteady pressures are very often measured by pneumatic probes connected with transducer faces by means of comparatively long bores or tubes of small diameter.

The relation between the time-dependent pressure at the probe inlet and at the transducer face depends on the characteristics of the pressure-wave propagation through the connection tubes. Determination of the time-averaged pressure is also an essential problem to be solved, especially when the relative amplitude of the pulsating pressure at the tube inlet is significant.

If the probe entrance were not influenced by the external gas stream, the time-averaged pressure at this place would be P_0, which is called the true time-averaged pressure at the measurement point. It is well known that the steady pressure occurring at the end of the transmission line does not represent the true time-averaged pressure at the probe port.[1-5] When the external stream velocity amplitude (Mach number) at the probe inlet is small, total pressure differences may be caused only by significant flow direction variations. Such a problem was presented in Ref. 5. The subject of this paper is different. The averaged pressure differences are caused by significant amplitudes of the total pressure at the probe inlet at high subsonic velocity of the external gas stream. The external gas stream is directed parallel to the measuring tube axis, and the angle of the stream variations is very small. The examples discussed in this paper refer to the total pressure-measuring system investigation in the experimental work by Krause et al.[3]

Received May 6, 1988; revision received Nov. 21, 1988.

*Professor, Fluid Mechanics.
†Research Scientist.

The comparison between theoretical results obtained using the method proposed here and experiments reported in Ref. 3 shows that the differences between the steady pressure at the end of the transmission line and the true time-averaged pressure at the measurement point can be composed of two parts.

The first one is due to the laminar oscillating gas motion effects inside the small-diameter long tube according to the model described in Ref. 1. The second part is due to the entrance effects. These effects are connected with the following: 1) the flow in the entrance segment of the tube (the entrance segment effect) with developing, unsteady, probably turbulent boundary layers, which differs significantly from the model proposed in Ref. 1. The entrance segment phenomena may take place at both sides of the first tube if it is connected to the second tube of a larger diameter, and 2) the interaction between the oscillating gas inside the tube at its inlet and the external pulsating gas stream flowing toward the probe tip (the entrance interaction effect).

It has been realized that the entrance effects lead to a pressure rise with respect to P_0 at the tube inlet.

An example of the entrance interaction has been introduced by Tijdeman[6] for a static pressure-measuring system. In the case discussed in Ref. 6, the oscillating airstream leaving the tube has to displace an external steady gas stream blowing across the static pressure tube entrance. This leads to an additional oscillatory pressure at the probe entrance determined semiempirically in Ref. 6.

The entrance phenomena occurring in the total pressure measuring system discussed here are more complicated than that described in Ref. 6. A more detailed explanation of the phenomena mentioned in points 1 and 2 above will be given below. It may be expected that for a very long, strongly damping tube, the contribution of the entrance effects to the time-averaged pressure at the tube end will be negligibly small. This will be confirmed in the fourth section of the paper.

Calculation Method

The method is based on the model described in Ref. 1 for the flow inside long tubes of small diameter. The entrance effects, which often play a very important role in total pressure measuring systems, will be introduced into the calculation procedure as the inlet boundary condition for time-averaged pressure.

The following assumptions are made following Ref. 1:
1) The tube radius R_j is very small compared with its length L_j.
2) The gas is viscous and heat-conducting.
3) The gas motion is unsteady, laminar, and axisymmetrical.
4) The pressure and temperature amplitudes are small with respect to their mean values.
5) The parameters μ, λ, C_p, C_v are constant.
6) The tube wall is isothermal with the temperature T_0. (The last two assumptions will be changed when a hot gas and cooled transducer are considered.)
7) The gas temperature in the transducer volume V at the tube end is constant and equal to T_0.

The inlet pressure wave (not disturbed by the entrance interaction) is different from that assumed in Ref. 1 and is presented as the Fourier series:

$$P_{,1}(0,t) = P_0 + Re\left[\sum_{k=1}^{\infty} \Delta P^k_{1z,1}(0) e^{ik\Omega}\right] \tag{1}$$

The small parameter of the used perturbation method is defined as

$$\epsilon = |\Delta P^1_{1z,1}(0)|/P_0 \tag{2}$$

Introducing Eq. (2) into Eq. (1) and relating Eq. (1) to the true time-averaged pressure P_0, one obtains the nondimensional form of Eq. (1):

$$p_{,1}(0,\tau) = 1 + \epsilon Re\left[\sum_{k=1}^{\infty} p^k_{1z,1}(0) e^{ik\tau}\right] \tag{3}$$

The nondimensional components of the first-order complex pressure perturbation amplitudes $p^k_{1z,1}(0)$ at the tube inlet are described by the formula

$$p^k_{1z,1}(0) = \Delta P^k_{1z,1}(0)/|\Delta P^1_{1z,1}(0)| \tag{4}$$

Usually five to ten harmonics are used in Eq. (3) for presentation of the inlet pressure wave shape.

Following Ref. 1, the boundary-layer equations and the perturbation method with the small parameter ϵ defined in Eq. (2) are used to find the solution of the problem.

The higher harmonics appearing in this expansion are introduced by assuming that the boundary-layer approach (used in Ref. 1) remains a valid approach to the problem.

This approach can be used if the boundary-layer thickness δ is much smaller than the wavelength ℓ. The nondimensional frequency ω^k_j (Ref. 1) defines the relation between the tube length L_j and the wavelength $\ell^k_j = L_j/\omega^k_j$. For $\omega = 0(1)$, it was estimated in Ref. 1 that $\delta^1_j/\ell^1_j = 0(R_j/L_j)$. Generally,

$$\delta = 0(R)$$

and so

$$R_j\omega^k_j/L_j \ll 1 \tag{5}$$

References 7 and 8 show that at high frequencies the boundary-layer thickness in the tube is proportional to $R_j/\sqrt{\omega^k_j}$. It occurs for the shear wave number [see Eq. (11)] $s^k_j > 20$. In this case, Eq. (5) is changed to the form

$$R_j\sqrt{\omega^k_j}/L_j \ll 1 \tag{6}$$

The criteria given above have to be satisfied for all harmonics appearing in the calculations.

First-order Perturbations

The solution of the first-order perturbation equations derived in Ref. 1 for the inlet impulse given by Eq. (3) can be presented as the following Fourier series for the pressure

$$p_{1,j}(\xi,\tau) = Re\left[\sum_{k=1}^{\infty} P^k_{1z,j}(\xi) e^{ik\tau}\right] \tag{7}$$

and similarly for the velocities $u_{1,j}$, $v_{1,j}$, density $\rho_{1,j}$, and the temperature $T_{1,j}$.

The harmonic components of the series expressed by Eq. (7) can be written based on the results described in Ref. 7. The complex amplitude of the first-order pressure perturbation is, for example,

$$p^k_{1z,j}(\xi) = G^k_{z,j}\, e^{-\Gamma^k_{z,j}(1-\xi)} + B^k_{z,j}\, e^{-\Gamma^k_{z,j}\xi} \tag{8}$$

where

$$\Gamma^k_{z,j} = \omega^k_j\left[\frac{\tau_o(i^{3/2}s^k_j)}{\tau_2(i^{3/2}s^k_j)}\frac{\kappa}{n^k_{z,j}}\right]^{1/2} \tag{9}$$

$$n^k_{z,j} = \left[1 + \frac{\kappa - 1}{\kappa}\frac{\tau_2(i^{3/2}s^k_j\sqrt{Pr})}{\tau_o(i^{3/2}s^k_j\sqrt{Pr})}\right]^{-1} \tag{10}$$

The nondimensional parameters defining the problem are

$$s^k_j = (\kappa K_j\omega^k_j)^{1/2}, \qquad K_j = \frac{P_0(R_j)^2}{\mu a_o L_j}, \qquad \omega^k_j = k\frac{\Omega L_j}{a_o} \tag{11}$$

The expressions for the complex amplitudes of the velocity perturbations $u^k_{1z,j}$, $v^k_{1z,j}$, the density and the temperature perturbations $\rho^k_{1z,j}$, $T^k_{1z,j}$, may be found in Refs. 7 and 9.

The complex constants $G^k_{z,j}$, $B^k_{z,j}$ are calculated from the boundary conditions for pressure specified in Refs. 7 and 9.

Time-averaged Pressure Perturbations

It can be proved that the second-order time-averaged pressure perturbation introduced in Ref. 1 may be generalized for the inlet pressure impulse given by Eq. (3) as

$$p_{20,j}(\xi) = \sum_{k=1}^{\infty} p^k_{20,j}(\xi) = \sum_{k=1}^{\infty} \left(16 \int \left\{ \frac{1}{K_j} \int_0^1 \overline{(\rho^k_{1,j} \cdot u^k_{1,j})} \eta \, d\eta + \kappa \int_0^1 \left[\phi^k_j(\xi,\eta) - \phi^k_j(\xi,1) \right] \eta \, d\eta \right\} d\xi + D^k_j \right) \tag{12}$$

where D^k_j are constants of the integration and

$$\phi^k_j(\xi,\eta) = \int \frac{1}{\eta} \left[\frac{\partial}{\partial \xi} \int \overline{(u^k_{1,j} \cdot u^k_{1,j})} \eta \, d\eta \right] d\eta + \frac{L_j}{R_j} \int \overline{(u^k_{1,j} \cdot v^k_{1,j})} \, d\eta \tag{13}$$

The overbars used in Eqs. (12) and (13) denote the time-averaged values of the products enclosed in the parentheses. These terms are calculated as

$$\overline{\sum_{k=1}^{\infty} (\rho^k_{1,j} \cdot u^k_{1,j})} = \frac{1}{2} \sum_{k=1}^{\infty} (\rho^k_{1c,j} \cdot u^k_{1c,j} + \rho^k_{1s,j} \cdot u^k_{1s,j}) \tag{14}$$

and similarly for the other products in Eqs. (12) and (13).

The components $p^k_{20,j}$ of the series (12) can be calculated according to the formula

$$p^k_{20,j}(\xi) = H^k_j(\xi) + D^k_j \tag{15}$$

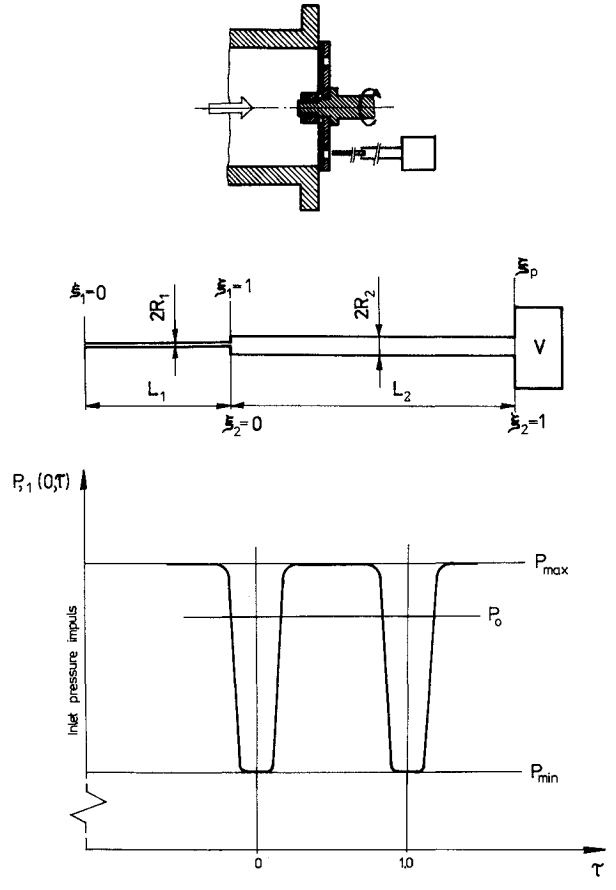

Fig. 1 Schematics of the test rig, tube systems, and inlet waveform of applied pressure.

where

$$H^k_j(\xi) = |p^k_{1z,j}(\xi)|^2 \cdot YA^k_j + \left| \frac{dp^k_{1z,j}(\xi)}{d\xi} \right|^2 \cdot YB^k_j + FP^k_j(\xi) \cdot YC^k_j$$

The expressions for YA^k_j, YB^k_j, YC^k_j, and $FP^k_j(\xi)$ come from Eqs. (12) and (13) and are given in Ref. 9.

The constants D^k_j (for a given harmonic k and for given tube segment $j = 1,2 \ldots n$) are calculated using boundary conditions for given time-averaged pressures at the tube inlet and at all consecutive tube connections.

At the tube inlet

$$D^k_1 = p^k_{20,1}(0) - H^k_1(0) \tag{16}$$

For each connection of the consecutive tubes, the equality of pressure leads to the following conditions:

$$p^k_{20,j}(1) = p^k_{20,j+1}(0) \qquad \text{for} \qquad j = 1,2,3 \ldots n \tag{17}$$

hence, D^k_{j+1} can be calculated as

$$D^k_{j+1} = H^k_j(1) - H^k_{j+1}(0) + D^k_j \tag{18}$$

and the computation of the time-averaged pressure perturbations for each tube segment is completed.

The time-averaged pressure at the tube inlet $p_{20,1}(0)$ [Eq. (16)] would be equal to zero if no second-order entrance effects were present at the tube entrance.

If the entrance effects (proportional to ϵ^2) are present at the tube inlet, $p_{20,1}(0)$ is not equal to zero, and the procedure of its determination is formulated in the next section of this paper.

Entrance Effects

The time-averaged total pressure recorded experimentally in Ref. 3 will be the subject of the theoretical calculations performed in this paper. The total pressure tubes used in the experiments described in Ref. 3 were located downstream of a nonsteady flow generator simulating turbomachinery flow conditions. The scheme of the generator, probes, and the total pressure inlet wave shape are shown in Fig. 1. The generator consists of a rotating wheel containing 20 nozzles of 8.2-mm exit diameter placed around a 70-mm-diam circle. The inlets of the total pressure tubes were placed about 2 diameters aft of the rotating wheel face.

The influence of the crossflow caused by the generator wheel rotation is neglected, because the crossflow velocity is very small compared to the velocity of the gas stream coming from the nozzles.

If $p_{20,1}(0) = 0$ is introduced into the time-averaged pressure calculations, then the typical results obtained for $P_{20,1}(1)$, when $K_1 \approx 10$, are shown in Fig. 7 by means of the dashed line. The experimental data taken from Ref. 3 are represented in the same figure by small crosses.

The theoretical curve deviates significantly from the experimental data. It can be explained that the differences between these two curves are caused by the entrance effects, which cause the time-averaged pressure to rise in the region of the entrance segment of the tube. For low values of K_1 (long, strongly damping tubes), the entrance effects are very small compared to the effects calculated according to Ref. 1, and these differences between theory and experiment disappear (see Fig. 4 for $K_1 = 2.72$).

The main reason for the entrance pressure rise is the character of the flow in the entrance segment of the tube. The entrance flow may be described as composed of compressible, nonsteady, developing, probably turbulent boundary layers and an oscillating inviscid core flow. The energy conversion in the entrance segment, which leads to the time-averaged pres-

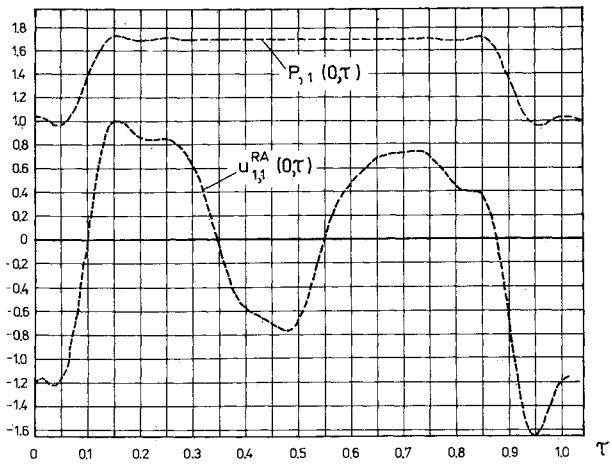

Fig. 2 External total pressure wave and internal velocity perturbations at the tube inlet during one period of oscillations, $IPD = 0.7$, $\beta = 0.75$, $\epsilon = 0.2055$, $\omega_1^1 = 0.4\Pi$.

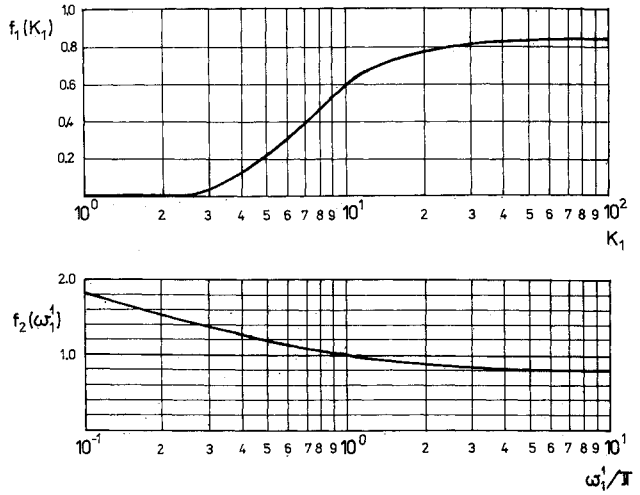

Fig. 3 Functions $f_1(K_1)$ and $f_2(\omega_1^1)$ determining the coefficient C_{20} in Eqs. (21) and (22).

sure rise, is much more intensive than that predicted by the flow model based on the perturbation method used in Ref. 1. The entrance phenomena may take place at both sides of the first tube of a smaller diameter (see Fig. 1).

Simplified numerical simulation of the oscillating flow formation mentioned above confirmed qualitatively that the entrance effects cause a distinct rise of the time-averaged pressure at the tube end.

Additionally, collisions between the internal gas stream periodically leaving the tube opening and the main external stream directed toward the probe inlet are the reason for the entrance pressure rise. The diagrams of the time-dependent total pressure of the external stream coming from the rotating nozzles and the internal velocity perturbations at the tube entrance are given in Fig. 2. The internal velocity perturbations $u_{1,1}^{RA}(0,\tau)$ (shown in Fig. 2) are calculated according to the model based on Ref. 1 and 7 and show only a qualitative illustration of the entrance phenomena. The negative value of $u_{1,1}^{RA}(0,\tau)$ means that the internal stream is directed outside of the tube entrance (see Fig. 2). It has been stated that the abovementioned interaction causes a time-averaged pressure rise at the tube inlet when $K_1 > 3$, and the nondimensional frequency is comparatively low $\omega_1^1 < 2\pi$.

The described entrance phenomena involve very complicated unsteady, viscous, compressible flows. The global semiempirical description of these effects is proposed in this paper. The effects of the entrance phenomena are introduced as the time-averaged pressure rise at the tube entrance $\xi_1 = 0$ and are represented by the inlet boundary condition $p_{20,1}(0)$ in Eq. (16).

The entrance effects cause a part of the kinetic energy of the main external gas stream to be converted into the time-averaged pressure rise. The numerous estimations allow the assumption that this pressure rise is proportional to the following part of the main stream kinetic energy:

$$\Delta P_{20,1}(0) \sim \frac{\rho}{2}(\epsilon W)^2 \tag{19}$$

where W is the maximum velocity of the external gas stream corresponding to the isentropic expansion in the generator nozzles.[3] Equation (19) shows that the pressure rise is treated as a second-order effect proportional to ϵ^2. The energy conversion takes place in the region of the flow where the thermodynamic parameters of a gas are close to the stagnation parameters and, therefore, ρ_o is used in Eq. (19). Introducing the proportionality coefficient C_{20} into Eq. (19) and relating the equation to P_o, the nondimensional relation can be derived:

$$\frac{\Delta P_{20,1}(0)}{P_o} = \epsilon^2 C_{20}\kappa\left(\frac{W}{a_o}\right)^2 \tag{20}$$

Taking into account that $\Delta P_{20,1}(0)/P_o = \epsilon^2 p_{20,1}(0)$, the entrance pressure rise is expressed in terms of its perturbation

$$P_{20,1}(0) = C_{20}\kappa\left(\frac{W}{a_o}\right)^2 \tag{21}$$

The proportionality coefficient C_{20} has been determined based on the experiments reported in Ref. 3. It was found that C_{20} is a function of K_1 and the nondimensional frequency ω_1^1 $C_{20}(K_1,\omega_1^1)$ is expressed in very simple form as a product of two functions of the separated arguments $f_1(K_1)$ and $f_2(\omega_1^1)$:

$$C_{20}(K_1,\omega_1^1) = f_1(K_1,) \cdot f_2(\omega_1^1) \tag{22}$$

The functions $f_1(K_1)$ and $f_2(\omega_1^1)$ are plotted in Fig. 3.

The function $f_1(K_1)$ has been determined using the experimental results given in Ref. 3 for $K_1 = 2$, 2.72, 5, 7.73, 9.39, 10.02, 11.69, and 39.7, and so this function will need further validation in the region of $K_1 > 15$.

Results and Comparisons

The experimental results reported in Ref. 3 are the only available data that may be used for comparisons with the theoretical calculations performed here. The averaged total pressure at the second tube end (Fig. 1) given in Ref. 3 is defined as $(P_{ind} - P_{true})/P_{true}$. This term, which may be called the total pressure correction, is identical to $\epsilon^2 p_{20,2}(1)$. The comparisons with the experiments will be performed for the time-averaged pressure perturbations $p_{20,2}(1)$. The small parameter ϵ is quoted for each investigated case in the figure captions, so that the total pressure corrections can be easily determined. The inlet total pressure profile (Fig. 1) is defined in Ref. 3 by P_{max}, P_{min}, and β.

The values of $(P_{max} - P_{min})/P_{min} = IPD$, and

$$\beta = (P_0 - P_{min})/(P_{max} - P_{min}) \tag{23}$$

are given for each case under consideration. The P_{min} is assumed after Ref. 3 as equal to the ambient pressure. The inlet total pressure wave shape duplicates that given in Ref. 3 as far as possible. It should be noted that β only varies between 0.7 and 0.8.

The measuring system consists of two consecutive tubes (Fig. 1). The first tube geometry is specified in Figs. 4–10. The second tube is much larger than the first one and only plays the role of a large volume in the tube system.

The results of the calculations with no entrance effects, i.e., for $p_{20,1}(0) = 0$, are plotted in Figs. 4–10 using dashed lines.

The results with the entrance effects introduced are presented by solid lines. The experimental data taken from Ref. 3 are shown by small crosses connected by thin lines.

Figures 4 and 5 are devoted to the cases of long, strongly damping tubes for which the entrance effects should play a negligibly small role. The results given in Figs. 4 and 5 confirm this expectation. The discrepancies observed for the first resonant frequencies might be analyzed if more details were known about the measuring test rig.

Figures 6–10 present the cases for which the entrance effects have to be introduced into the calculation procedure. It can be seen that the results of the calculations are in good agreement with the experiment when $p_{20,1}(0)$ is determined according to the semiempirical relation given by Eq. (21). However, the analysis of Fig. 8 suggests that the function $f_2(\omega_1^1)$ probably has a more complicated form and depends additionally on $L_1/2R_1$ for low frequencies. This correlation would be possible if more experimental data were available.

The results presented in Figs. 6–9 concern oscillating flows inside the tube, which are laminar at a distance from the tube inlet. In the region of the entrance segments the flows may be turbulent, but this eventuality was included in the entrance effect model. The results plotted in Fig. 10 refer to the turbulent flow inside the whole tube in the presence of a resonant frequency. The mean Reynolds number in the resonant fre-

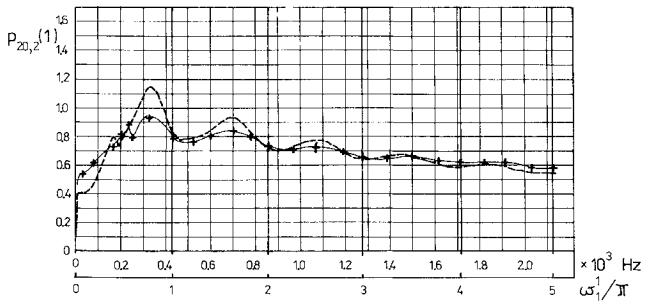

Fig. 4 Comparison with experiment Ref. 3 for $R_1 = 0.21$ mm, $L_1 = 0.4$ m, $K_1 = 2.72$, $IPOD = 0.7$, $\beta = 0.75$, $\epsilon = 0.2055$.

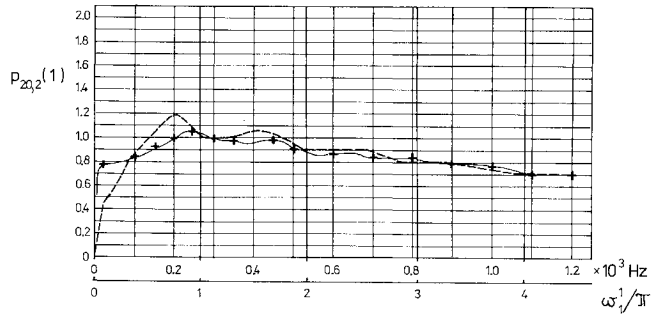

Fig. 5 Comparisons with experiment Ref. 3 for the tube of $L_1 = 0.63$ m filled with a bundle of fine wires, $K_1 \approx 2.0$, $IPD = 0.68$, $\beta = 0.75$, $\epsilon = 0.202$.

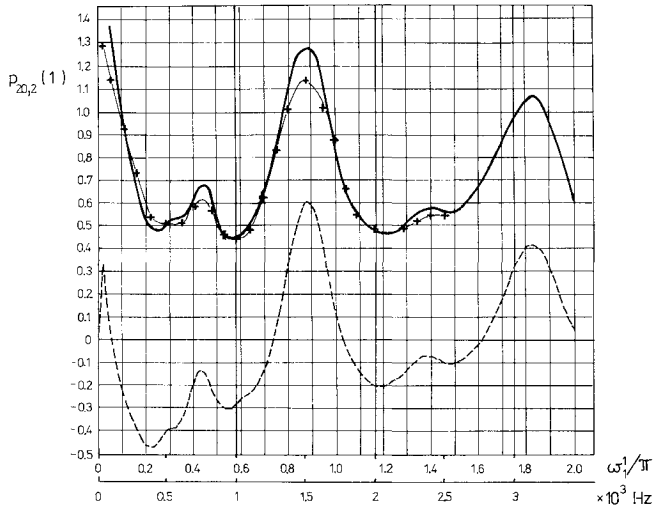

Fig. 6 Comparisons with experiment Ref. 3 for $R_1 = 0.21$ mm, $L_1 = 0.1$ m, $K_1 = 11.69$, $IPD = 0.85$, $\beta = 0.75$, $\epsilon = 0.232$.

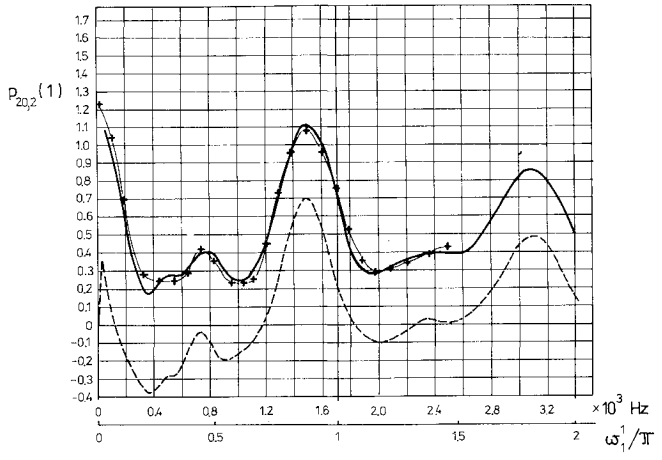

Fig. 7 Comparisons with experiment Ref. 3 for $R_1 = 0.21$ mm, $L_1 = 0.1$ m, $K_1 = 9.39$, $IPD = 0.42$, $\beta = 0.75$, $\epsilon = 0.135$.

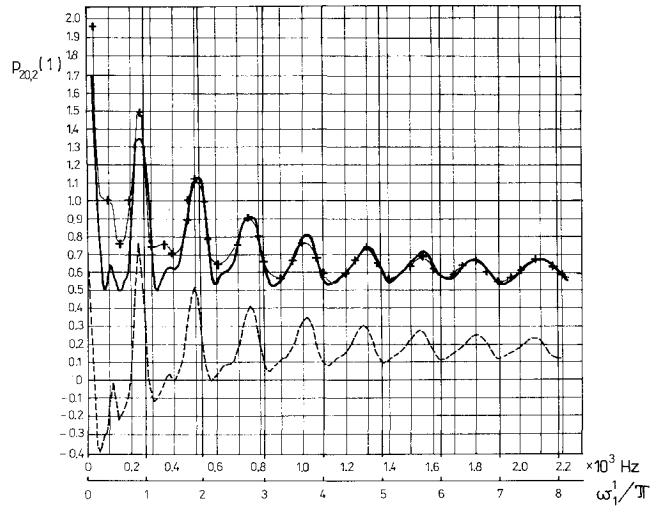

Fig. 8 Comparisons with experiment Ref. 3 for $R_1 = 0.5$ mm, $L_1 = 0.63$ m, $K_1 = 10.02$, $IPD = 0.70$, $\beta = 0.79$, $\epsilon = 0.167$.

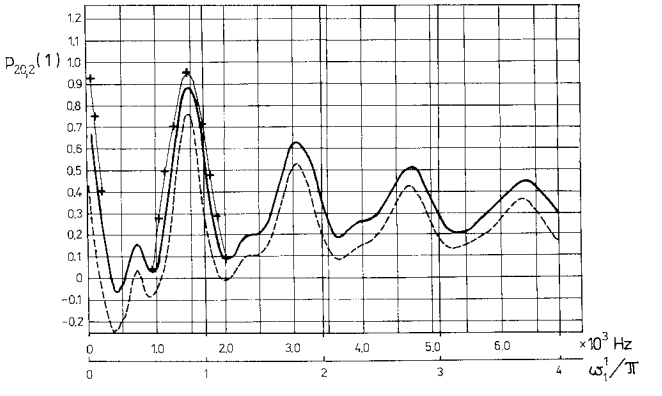

Fig. 9 Comparisons with experiment Ref. 3 for $R_1 = 0.21$ mm, $L_1 = 0.1$ m, $K_1 = 7.73$, $IPD = 0.11$, $\beta = 0.75$, $\epsilon = 0.0455$.

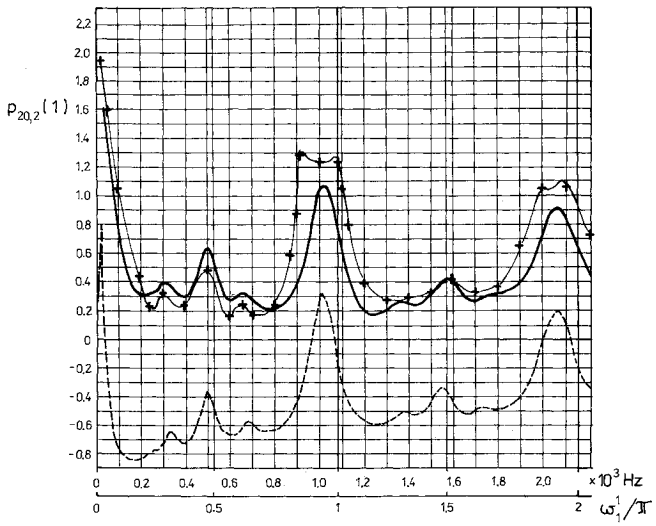

Fig. 10 Comparisons with experiment Ref. 3 for $R_1 = 0.5$ mm, $L_1 = 0.159$ m, $K_1 = 39.7$, $IPD = 0.7$, $\beta = 0.8$, $\epsilon = 0.174$.

quency bands are about 10^4. The discrepancies between the theory and experiments appearing in Fig. 10 for resonant conditions are caused by the turbulence.

Figure 9 presents the comparison for the case of the lowest values of the relative inlet total pressure difference $(P_{max} - P_{min})/P_{min} = IPD = 0.11$. The relative maximum velocity at the tube inlet $W/a_o = 0.39$. The maximum value of the total pressure correction is lower than 0.002 for this case. The entrance effects, proportional to $(W/a_o)^2$, are very small as well. It can be estimated from Fig. 9 where entrance effects are illustrated by the distance between the dashed and solid lines.

Conclusions

The total time-averaged pressure corrections for the pressure-measuring tube system are substantial when the amplitudes of the pulsating total pressure at the probe inlet are significant. The external gas stream is directed parallel to the measuring tube axis and the angle of the stream variations is very small. The analysis presented in this paper shows that the total time-averaged pressure corrections may be neglected if the relative inlet total pressure differences $(P_{max} - P_{min})/P_{min} < 0.2$. It should be noted that this conclusion is valid only when all conditions concerning the flow mentioned in this paper are fulfilled.

The calculation method is based on the solution described in Ref. 1. For long, strongly damping tubes ($K_1 < 3$), the theoretical results of Ref. 1 reveal good agreement with the experiments reported in Ref. 3 (see Figs. 4 and 5). For tubes with reduced damping, the method had to be supplemented by a procedure that accounts for the entrance effects. These effects produce an pressure rise, which was introduced in the calculation method as the boundary condition. The comparisons with experiment are satisfactory.

The results shown in Figs. 6–9 concern flows that are laminar inside the tube at a distance from the inlet. In the entrance region, the flow is more complex, which is included in the entrance effects model. The results shown in Fig. 10 refer to the flow that is turbulent in the whole tube for the resonant frequency bands [$Re = 0(10^4)$]. The discrepancies shown in Fig. 10 for the resonant regions are caused by the turbulence.

The investigations of the turbulent pulsating flows in tubes[10] show that the velocity profiles in turbulent and laminar pulsating flows show a flat inner core of essentially the same extent, although the amplitude of the turbulent flow velocity is a little lower [$Re = 0(10^4)$, $S_1^1 \simeq 70$]. The experiment reported in Ref. 10 reveals, in addition, that the unsteady wall shear stress in turbulent flow for $S_1^1 \simeq 70$ is about 13% higher and for $S_1^1 \simeq 140$ about 20% higher than in laminar flow, with no phase shift. These facts explain the moderate discrepancies between the theoretical and experimental results observed in Fig. 10.

The results presented in Fig. 9 show that the time-averaged pressure corrections are very small when the total pressure amplitude at the tube inlet is moderate. However, for significant amplitudes, the value of the maximum pressure corrections ranged up to 6% (see Fig. 6).

Organ pipe resonances are very well predicted by the theoretical calculations. During resonances the pressure corrections increase significantly. The resonance amplitudes could be reduced by application of long, strongly damping tubes. However, the level of the time-averaged pressure correction rises considerably in the inter-resonance regions for such tubes.

References

[1]Kazimierski, Z. and Trojnarski, J., "Time-Averaged Pressure of Fluctuating Gas Motion in Small-Diameter Tubes," *AIAA Journal,* Vol. 25, April 1987, p. 567.

[2]Weyer, H., "Bestimung der zeitlichen Druckmittelwerte in stark fluktuierender Stroemung: insbesondere in Turbomaschinen," German Aerospace Research Establishment, DFVLR FB 74-34, 1974.

[3]Krause, L. N., Dudzinski, T. J., and Johnson, R. C., "Total Pressure Averaging in Pulsating Flows," *ISA Trans.,* Vol. 13, No. 2, 1974.

[4]Kronauer, R. E. and Grand, H. P., "Pressure Probe Response in Fluctuating Flow," *Proceedings of 2nd U.S. National Congress of Applied Mechanics,* American Society of Mechanical Engineers, New York, 1954.

[5]Samoilovič, G. S. and Yablokov, L. D., "Measurement of Periodically Fluctuating Flows in Turbomachines by Ordinary Pitot Tubes," *Izmierienie periodičrdki pulsinieuščich potokov v turbomašinach Tieploenergietika,* Vol. 17, No. 9, Sept. 1970, p. 70.

[6]Tijdeman, H., "Investigations of the Transonic Flow Around Oscillating Airfoils," Ph.D. Thesis, Delft Technological University, National Aerospace Laboratory, Amsterdam, TR 77090U, Oct. 1977.

[7]Tijdeman, H., "On Propagation of Sound Waves in Cylindrical Tubes," *Journal of Sound and Vibrations,* Vol. 24, Jan. 1975, p. 1.

[8]Telionis, D. P., "Unsteady Viscous Flows," Springer-Verlag, New York, 1981.

[9]Kazimierski, Z., "Time-Averaged Pressure of Fluctuating Gas Motion in Small-Diameter Tubes for Non-Harmonic Inlet Impulses," *Proceedings of IV International Symposium, Sept. 6-10, 1987 on Unsteady Aerodynamics and Aeroelasticity of Turbomachines,* RWTH Aachen, Templergraben 55, 5100 Aachen, FRG, Mitteilung Nr 8-01, p. 707.

[10]Emsmann, S., "Experimentelle Ermittlung der Geschwindigkeitsverteilung in einer oszillierenden turbulenten Rohrströmung," Ph.D. Thesis, Technical University of Berlin, FRG, 1973.